Impact of clay minerals on reservoir sandstone properties: comparative study in Colombian eastern cordillera and middle Magdalena valley basins

Fred Jesús Paba-Santiago[1]
✉ Carlos Alberto Ríos-Reyes[1]
Hernando Buendía-Lombana[1]

1. Universidad Industrial de Santander, Colombia

✉ *Autor de correspondencia:*

Carlos Alberto Ríos-Reyes
Geólogo, PhD
Universidad Industrial de Santander,
Colombia
carios@uis.edu.co

Abstract

The aim of this study is to examine how mineralogy influences the petrophysical properties, particularly porosity and permeability, of potential sandstone reservoirs in Colombia. It seeks to comprehensively understand how the presence of clay minerals impacts the overall quality of hydrocarbon reservoirs in the country. Samples of sandstones from reservoirs at various outcrops in the Eastern Cordillera and Middle Magdalena Valley basins were collected. Detailed analysis of mineralogy and petrographic characteristics of the samples was conducted through various analytical techniques such as transmitted light microscopy, X-ray diffraction, and scanning electron microscopy. Porosity and permeability were measured using automated permeametry and porosimetry equipment. The predominant composition of the analyzed reservoir rocks comprises quartz (45-50%), feldspar (35-40%), and clays (10-20%). These rocks were categorized into two distinct groups based on their permeability (K) and porosity (Φ), ranging from 0.009 to 29.220 mD and 1.88 to 20.75%, respectively. The presence of illite correlated with a reduction in both porosity and permeability, highlighting its negative impact on reservoir quality. Conversely, an elevated concentration of kaolinite was associated with favorable porosity and permeability. Samples with feldspar sericitization demonstrated inferior hydrocarbon storage quality. This study provides a deeper understanding of how mineralogy affects the petrophysical properties of sandstone reservoirs in Colombia. These findings are crucial for guiding exploration and production strategies in the Colombian oil industry, especially in challenging geological environments like those studied.

Keywords: clay minerals; mineralogy; petrography; petrophysical properties; porosity; permeability; sandstone reservoirs; sedimentary basins; oil industry; Colombia

Impacto de minerales arcillosos en propiedades petrofísicas de los reservorios de areniscas: estudio comparativo en las cuencas de la cordillera oriental y el valle medio del Magdalena (Colombia)

Resumen

El objetivo de este estudio es examinar cómo la mineralogía influye en las propiedades petrofísicas, especialmente la porosidad y permeabilidad, de posibles reservorios de arenisca en Colombia. Busca comprender de manera integral cómo la presencia de minerales arcillosos afecta la calidad general de los reservorios de hidrocarburos en el país. Se recolectaron muestras de areniscas de reservorios en varios afloramientos en las cuencas de la Cordillera Oriental y el Valle del Magdalena Medio. Se realizó un análisis detallado de la mineralogía y características petrográficas de las muestras mediante diversas técnicas analíticas como microscopía de luz transmitida, difracción de rayos X y microscopía electrónica de barrido. La porosidad y permeabilidad se midieron utilizando equipos automatizados de permeametría y porosimetría. La composición predominante de las rocas de los reservorios analizados comprende cuarzo (45-50%), feldespato (35-40%) y arcillas (10-20%). Estas rocas se clasificaron en dos grupos distintos según su permeabilidad (K) y porosidad (Φ), que van desde 0.009 hasta 29.220 mD y del 1,88 al 20,75%, respectivamente. La presencia de ilita se correlacionó con una reducción tanto en la porosidad como en la permeabilidad, destacando su impacto negativo en la calidad del reservorio. Por el contrario, una concentración elevada de caolinita se asoció con una porosidad y permeabilidad favorables. Las muestras con sericitización de feldespato demostraron una calidad de almacenamiento de hidrocarburos inferior. Este estudio proporciona una comprensión más profunda de cómo la mineralogía afecta las propiedades petrofísicas de los reservorios de arenisca en Colombia. Estos hallazgos son cruciales para guiar las estrategias de exploración y producción en la industria petrolera colombiana, especialmente en entornos geológicos desafiantes como los estudiados.

Palabras claves: minerales arcillosos; mineralogía; petrografía; propiedades petrofísicas; porosidad; permeabilidad; reservorios de arenisca; cuencas sedimentarias; industria petrolera; Colombia

1. Introduction

Clay minerals exert a substantial influence on the assessment of both the quality and petrophysical properties of sandstone reservoirs at a global scale. The widespread existence of clay minerals introduces considerable challenges, notably impacting the comprehensive understanding of these reservoirs (e.g., Islam, M.A. 2009; Al-Kharra'a et al., 2023; Risha et al., 2023). The presence of authigenic clay minerals profoundly influence the pore geometry of clastic reservoirs, thereby exerting significant effects on drilling and hydrocarbon production (Samakinde et al., 2016). According to Anovitz and Cole (2015), porosity and permeability are the most important properties in reservoir rocks, which control fluid storage and fluid flow behaviors, respectively. Porosity is closely related to the reservoir storage capacity, whereas permeability controls the seepage process (Zhao et al., 2015). The characteristics of the pore space such as porosity and permeability are the key factors that affect the reservoir exploitation (Ghanizadeh et al. 2015) and, therefore, they are most important for the weathering behavior of sandstones (e.g., Putnis and Mauthe, 2000). On the other hand, an accurate petrophysical data and an accurate understanding of the controlling factors of porosity and permeability are crucial for the successful exploitation of oil reservoirs. Several techniques have been widely used in the characterization of petrophysical properties of reservoirs, which include computed tomography (CT) (e.g., Pini et al., 2012; Desbois et al., 2016; Zhang et al., 2016), micro-computed tomography (micro-CT) (e.g., Bera et al., 2011; Landrot et al., 2012; Shah et al., 2016; Desbois et al., 2016; Kweon and Deo, 2017; Kareem et al., 2017), scanning electron microscopy (SEM) (e.g., Combes et al., 1998; Landrot et al., 2012; Lai et al., 2015; Desbois et al., 2011, 2016; Kareem et al., 2017), Quantitative Evaluation of Minerals by Scanning Electron Microscopy (QEMSCAN) (e.g., Sliwinski et al., 2010; Kweon and Deo, 2017), Focused Ion Beam Scanning Electron Microscopy (FIB-SEM) (e.g., Bera et al., 2011; Landrot et al., 2012; Desbois et al., 2016), Broad Ion Beam Scanning Electron Microscopy (BIB-SEM) (e.g., Desbois et al., 2011, 2016), Nuclear magnetic resonance (NMR) (e.g., Rosenbrand et al., 2015), X-ray

diffraction (XRD) (e.g., Kassab et al., 2017; Kareem et al., 2017) or mercury injection porosimetry (MIP) (e.g., Matthews et al., 1995; Rosenbrand et al., 2015; Campos et al., 2015; Kareem et al., 2017). However, there is still a great deal of knowledge between having the reservoir quality data and understanding the effects of clay minerals on petrophysical properties. The pore-size distribution, clay particle sizes, the distribution of the clays within the pore space and the composition of the clays are all-important factors in controlling porosity and permeability of reservoirs. Clay minerals as primary matrix, pseudomatrix and/or later infiltration phases into open pore spaces is a significant problem of sandstones with regard to their weathering stability, since they considerably influence porosity and permeability (Houseknecht and Pittman 1992). Neoformation, transformation and alteration of different clay minerals define them as a special parameter in sandstones that requires careful analysis when characterizing the material behavior of a sandstone (Stück et al., 2013a). Understanding how all these factors affect porosity and permeability is an arduous task. Fortunately, the diagenetic minerals within the sandstones provide simple ways to determine the overall effects of the complex compaction and diagenesis processes on the petrophysical properties. The Eastern Cordillera and Middle Magdalena Valley basins in Colombia host oil reservoirs characterized by complexity and tight formations, making it challenging to predict their accumulation mechanisms. These basins exhibit medium petroleum maturity, strong diagenesis, fine to medium-sized rock particles, effective calibration, high cement content, and significant heterogeneity (e.g., Schamel, 1991; Cooper et al., 1995; García et al., 2009, Aguilera et al., 2010; Caballero et al., 2010). The intricate relationship between clay minerals and petrophysical properties emphasizes the importance of a comprehensive understanding of mineralogical compositions, diagenetic processes, and pore structures. This understanding is crucial for enhancing reservoir characterization and optimizing exploration and production strategies in challenging geological environments.

2. Materials and analytical methods

The reservoir sandstones examined in this study were collected from various outcrops located in the Eastern Cordillera and Middle Magdalena Valley basins. Six core plugs, each measuring 2.5 cm in diameter and 5 cm in length, were extracted from hand specimens using a pneumatic drill at the Geological Samples Preparation Laboratory of the School of Geology, Universidad Industrial de Santander. Additionally, thin section preparation for petrographic analyses was carried out at the same laboratory. A preliminary visual inspection of the core plugs was performed through a binocular Zeiss stereomicroscope (model Stemi DV4) to distinguish their textural and macrostructural features. Petrographic analysis was carried out by transmitted light microscopy, using a Leica DM750P transmitted light microscope. Thin sections were initially inspected in order to obtain preliminary information on parallel and crossed nicols, which is essential to facilitate the location of sites of interest for obtaining microphotographs, determining their textural parameters. Then, the rock samples were analyzed by X-ray powder diffraction (XRPD) and field emission gun-environmental scanning electron microscopy/energy dispersive X-ray spectroscopy (FEG-ESEM/EDS). Bulk mineralogical composition was determined via XRPD using a BRUKER D8 ADVANCE X-ray diffractometer equipped with operating in Da Vinci geometry and equipped with an X-ray tube (Cu-Kα1 radiation: λ = 1.5406 Å), a 1-dimensional LynxEye detector (with aperture angle of 2.93º), a divergent slit of 0.6 mm, two soller axials (primary and secondary) of 2.5º and a nickel filter. All samples were milled in an agate mortar to a particle size of less than 50 μm and then mounted on a sample holder of polymethylmethacrylate (PMMA) using the filling front technique prior to XRPD analysis. Data collection was carried out at 40 kV and 30mA in the 2θ range of 3.5-70°, with a step size of 0.01526° (2θ) and counting time of 1 s/step. Phase identification was performed using the crystallographic database Powder Diffraction File (PDF-2) from the International Centre for Diffraction Data (ICDD) and the Crystallographica Search-Match program. The unit-cell constants, atomic positions, factors of peak broadening and phase concentrations were refined and

calculated by using the MDI RIQAS program based on Rietveld method. The pore morphology of both freshly broken and polished surfaces of samples was observed using FEI QUANTA 650 FEG-ESEM, under the following analytical conditions: magnification = 100-20000x, WD = 9.0-11.0 mm, HV = 20 kV, signal = BSE in ZCONT mode, detector = BSED, EDS Detector EDAX APOLO X with resolution of 126.1 eV (in. Mn Kα). All the samples were carbon coated for observation. Before the petrophysical analyses, the residual oil was removed from a plug, which were further dried under vacuum for 24 h. Porosity and permeability were first measured using an AP-608 automated permeameter and porosimeter. A fully automated Coreval 700 instrument of Vinci Technologies was used to measure the porosity and permeability to helium/nitrogen of the plug sized core samples at a confining pressure of 400 psi. The instrument is provided with a data acquisition and calculation computer station. Permeability measurements can be made using the unsteady state pressure drop method. These data were used to determine the equivalent liquid permeability, slip and turbulence factors. Equivalent air permeability at a user specified pressure is also computed. Porosity and pore volume measurements are made using the Boyle's and Charles' law technique. Rock compressibility factor, fracture volume and real pore volume can also be computed.

3. Results

3.1. Field occurrence

Figure 1 illustrates various aspects of the field occurrence of sandstone outcrops within the geological formations considered in this study, presented in chronostratigraphic order. In Figure 1a, a representative outcrop of sandstones from the Tibet Formation is shown, initially identified by Cediel (1969) as a Tibet Member, designating the sandy basal part of the Floresta Formation. The Floresta Formation comprises a sequence of sandstones, locally conglomerate, deposited in a fluvial environment on a steep paleotopography. Barret (1983) assigns a late Early Devonian age to the Tibet Formation. Figure 1b displays a typical outcrop of

sandstones from the Lower Member of the Tibasosa Formation. This member comprises a succession of fine- to coarse-grained quartz sandstones, occasionally conglomeratic, exhibiting colors that vary from light gray to white, greenish-gray, and reddish due to weathering. This unit dates back to the Late Jurassic and Early Cretaceous periods. Etayo-Serna et al. (1983) describe the Arcabuco Formation as thick quartz sandstone banks, occasionally conglomeratic, with light colors, sometimes reddish, containing layers of mudstones. Renzoni (1981) assigns a Late Hauterivian - Albian age to the Tibasosa Formation, while Alzate and Bueno (1994) extend the age range (Valanginian - Late Albian) based on ammonite paleofauna. The Tibasosa Formation overlays the Girón Formation with a faulty contact and underlies the Une Formation concordantly. In Figure 1c, a representative outcrop of the Arcabuco Formation is shown, consisting of thick beds of light-colored, quartz-rich sandstones and conglomerates with intermittent shales. This unit dates back to the Late Jurassic and Early Cretaceous periods. Etayo-Serna et al. (1983) describe the Arcabuco Formation as thick quartz sandstone banks, occasionally conglomeratic, with light colors, sometimes reddish, containing layers of mudstones. Scheibe (1938) originally described it as late Jurassic based on the fossil fauna, while Etayo-Serna (1968) assigns it an early Cretaceous age based on correlations with the overlying unit. Galvis and Rubiano (1985) propose that the Arcabuco Formation was deposited in a continental to transitional environment, possibly a deltaic plain. The Los Santos Formation is characterized by conglomerate sandstones, grayish-red mudstones, and yellowish-gray quartz sandstones with cross-stratification. These facies are interpreted as fluvial deposits accumulated by braided currents (Royero and Clavijo, 2001).
The lower contact is considered transitional and discordant with the Girón Formation, while the upper contact is concordant with the overlying Rosablanca Formation. Although Etayo-Serna and Rodríguez (1985) suggest a Berriasian age, Ward et al. (1973) assign a Valanginian-Hauterivian age based on fossil content. Los Santos Formation sandstones (Figure 1d) are exposed along outcrops with steep vertical slopes, mainly comprising conglomeratic sandstones, grayish-red mudstones, and quartz yellowish-gray sandstones with tabular geometry and cross-stratification. Figure 1e displays a

typical outcrop of sandstones from the lower member of the Picacho Formation. This formation has concordant and net contacts with the Socha Clays and Concentración formations (Ulloa et al., 2003) and likely formed in a fluvial environment of braided rivers or well-drained plains (Rodríguez and Solano, 2000). These sandstones are primarily white, fairly clean, massive, moderately hard to friable, fine- to coarse-grained, and may exhibit sedimentation structures such as current marks and cross-stratification. According to palynological studies by Vergara and Rodríguez (1997), the Picacho Formation is assigned an age from the Upper Paleocene.

Figure 1. (a) Outcrop of sandstones from the Tibet Formation overlying the Otengá Stock. (b) Cross-bedded Late Jurassic to Early Cretaceous sandstones of the Arcabuco Formation. (c) Tabular geometry in sandstones of the Los Santos Formation. (d) Interlayered sandstones and claystones of the Tibasosa Formation. (e) Vertical sandstone layers of the Picacho Formation, displaying a tabular geometry.

3.2. Detrital texture and composition

Detrital texture and composition are fundamental aspects in comprehending the geological and petrophysical characteristics of sandstone reservoirs. Figures 2-7 meticulously explore these crucial facets, providing an in-depth analysis of the textural and

microstructural attributes inherent in the examined sandstones. Macroscopic analysis has been instrumental in revealing notable differences among the sandstones, encompassing variations in weathering conditions, compactness, grain size, sphericity and roundness, color, and mineral composition. A closer examination of detrital texture unveils essential insights. Weathering conditions within the sandstones offer valuable information about their endurance and performance in diverse environmental settings. Variations in compactness provide insights into the porosity and permeability of the sandstones, crucial factors shaping fluid flow within reservoirs. The distribution of grain sizes, sphericity, and roundness contributes to our understanding of sedimentary processes and transport dynamics, offering essential information about the depositional environment and energy conditions during sedimentation. Color, another notable aspect, often reflects the mineral content and alteration processes, providing valuable insights into the diagenetic history of the sandstones. Furthermore, the mineral composition, a key determinant of reservoir quality, influences factors such as cementation and porosity. In the comprehensive evaluation of reservoir rock samples, transmitted light microscopy emerges as the preferred method, offering a straightforward, accurate, and repeatable means to assess not only the detrital texture but also the pore system and associated mineralogy. This analytical approach facilitates a nuanced understanding of the intricate relationships between detrital components and their impact on the physical and chemical properties of the reservoir, contributing to the characterization and potential exploitation of these geological formations. Specifically focusing on Figure 2 and examining sample TIB-1, we delve into its intricate features. Texturally, TIB-1 is classified as a sandstone, and compositionally, it falls into the category of a medium- to coarse-grained sandstone (lithic arkose). Notably, the sample exhibits a significant matrix between grains and displays high cementation, contributing to its overall compact appearance with minimal signs of oxidation. The fine-grained matrix is predominantly composed of clay minerals, while the rigid grains present sub-angular to sub-rounded shapes, suggesting a wide grain size distribution and indicating potential short transportation times. The larger grains, consisting

mainly of quartz, potassium feldspar, and plagioclase, exhibit feldspar alteration to sericite. Additionally, fractures are filled with oxides. The rock's cement is composed of feldspars, and its matrix consists of unstable minerals, underscoring the influence of the source area's climate and relief on its distinctive composition.

Figure 2. (a) Photograph of a non-polished slide of the plug of the sandstone TIB-1 and its characteristic texture under the stereomicroscope. (b)-(c)-(d) Photomicrographs in plane-polarized light and crossed-polarized light of the analyzed sandstone.
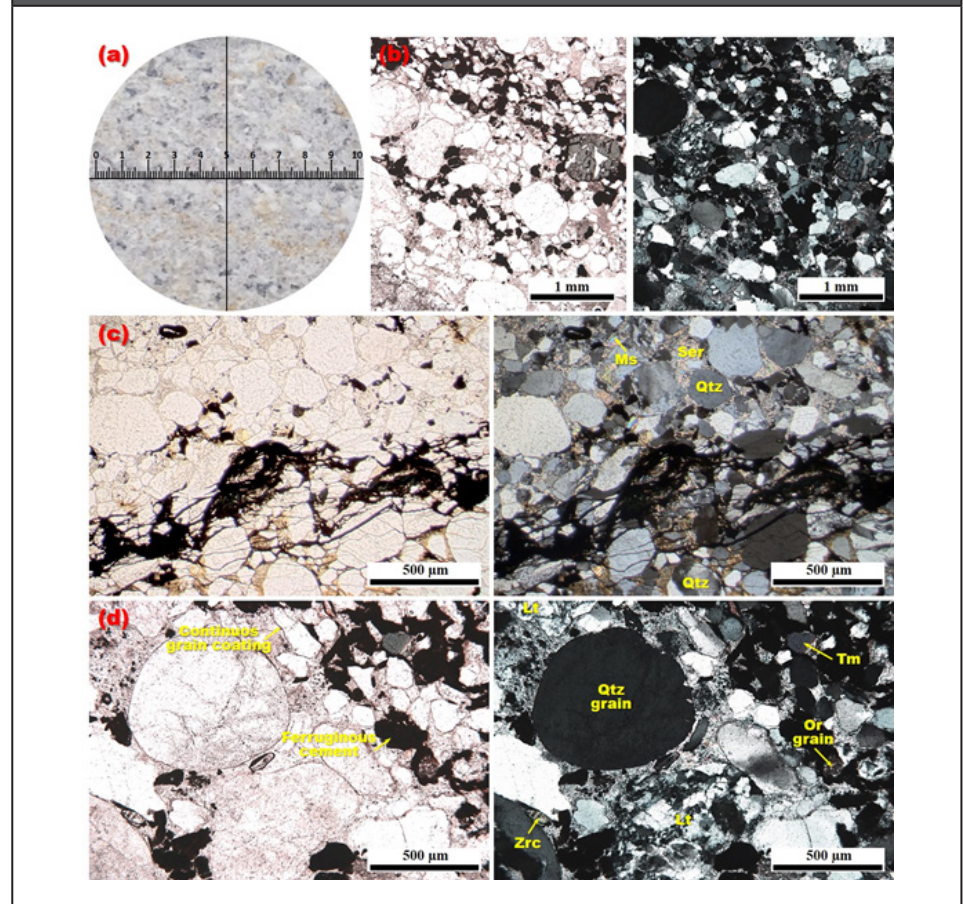
Figure 3 illustrates the characteristics of sample ARC-1, which is texturally classified as a sandstone and compositionally identified as a medium- to coarse-grained sandstone (lithic arkose). This sample exhibits a significant amount of clay matrix between grains, contributing to its overall tight appearance and high cementation. Notably, oxides are observed precipitated into fractures throughout the bulk of the rock, adding to its distinctive features. The rigid

grains in sample ARC-1 display a sub-angular to sub-rounded morphology, indicating a wide grain size distribution and suggestive of limited transport time from the source area (poor selection). The larger grains primarily consist of quartz and feldspars. Quartz, at times, exhibits wavy extinction patterns attributed to deformation. Additionally, a majority of feldspars show alteration to sericite, further contributing to the rock's mineralogical composition. Abundant cement, primarily composed of feldspar and silica, is evident within the rock. The presence of this cement, along with a matrix of unstable minerals, signifies the influence of the climate and relief of the source area on the rock's formation. The overall characteristics of sample ARC-1 provide valuable insights into the sedimentary processes, transportation dynamics, and diagenetic history, contributing to a more comprehensive understanding of the reservoir's physical and chemical properties.

Figure 3. (a) Photograph of a non-polished slide of the plug of the sandstone ARC-1 and its characteristic texture under the stereomicroscope. (b)-(c)-(d) Photomicrographs in plane-polarized light and crossed-polarized light of the analyzed sandstone.
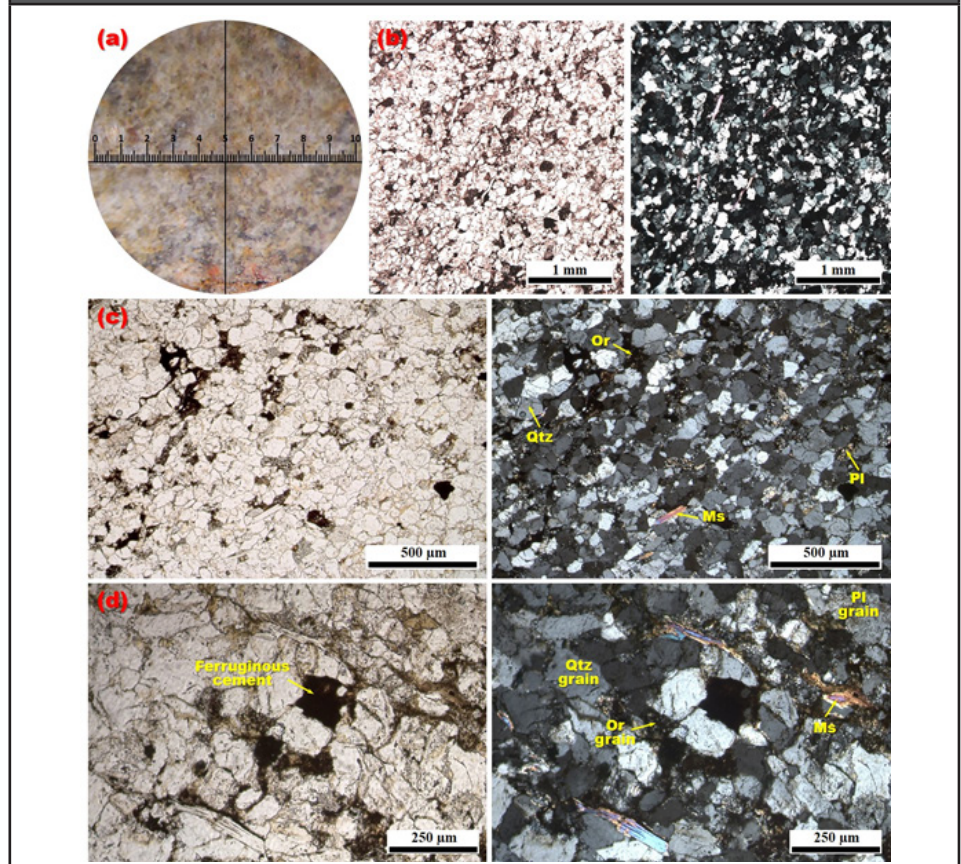
Figure 4 shows the characteristics of sample LSA-1, identified texturally as a sandstone and compositionally as a medium- to coarse-grained sandstone. This sample exhibits a significant presence of fine-grained clay matrix between grains, contributing to its overall tight appearance and high cementation. Notably, there is an absence of oxides in considerable amounts, further distinguishing its features. The rigid grains within sample LSA-1 are predominantly more or less sub-rounded, indicating a wide grain size distribution and suggesting relatively short transportation times (poor selection). The larger grains primarily comprise quartz and feldspars, with plagioclase being the dominant feldspar and a smaller amount of microcline. A substantial alteration of most feldspars to sericite is observed, to the extent of being confused with the matrix. Abundant cement, primarily composed of feldspar and silica, is evident in this rock. The matrix consists of unstable minerals, pointing towards the influence of the climate and relief of the source area on the rock's formation. The detailed examination of sample LSA-1 provides crucial insights into sedimentary dynamics, transportation processes, and diagenetic alterations, contributing significantly to our understanding of the reservoir's physical and chemical properties.

Figure 4. (a) Photograph of a non-polished slide of the plug of the sandstone LSA-1 and its characteristic texture under the stereomicroscope. (b)-(c)-(d) Photomicrographs in plane-polarized light and crossed-polarized light of the analyzed sandstone.
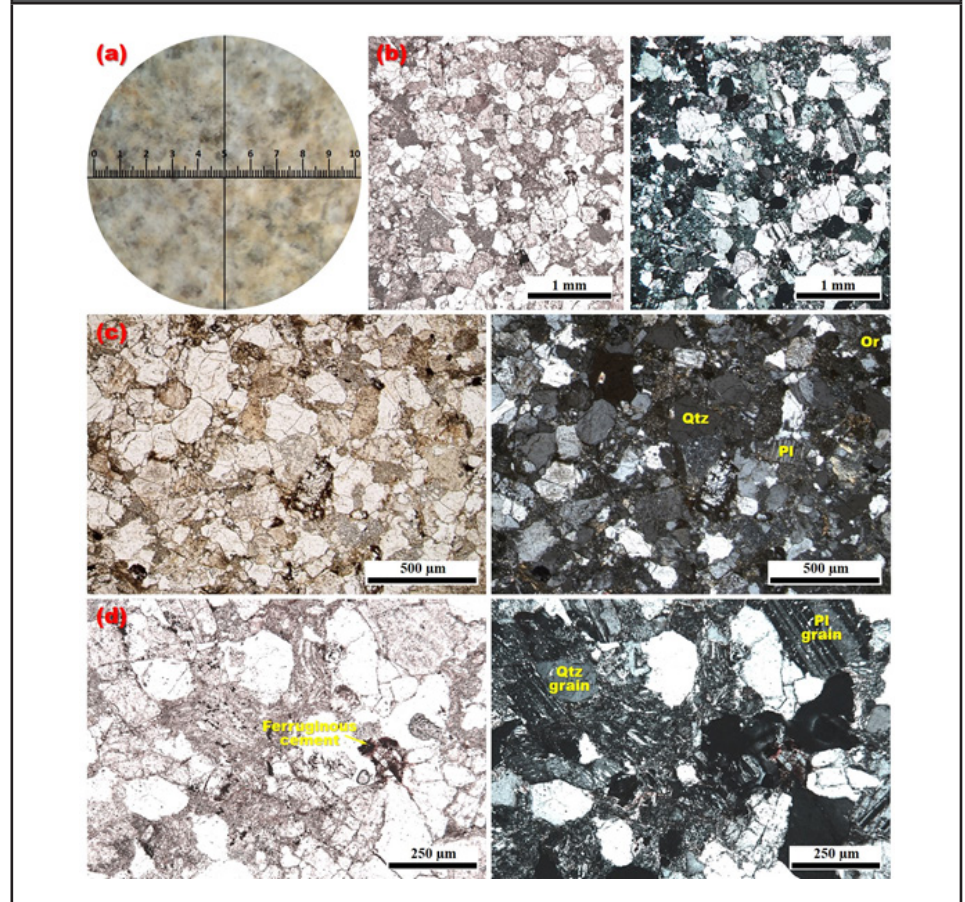
Figure 5 shows the characteristics of sample TBS-1, identified texturally as a sandstone and compositionally as a coarse-grained sandstone (subarkose). This sample features a significant amount of clay matrix between grains but exhibits relatively low cementation. Notably, there is a discernible tight appearance, and the presence of oxides is minimal. The rigid grains within sample TBS-1 are predominantly more or less subangular, indicating a wide grain size distribution (poor selection) and suggesting limited transport time from the source area, particularly of granitic origin. The rigid grains are composed of quartz, potassium feldspar, and a small amount of plagioclase. A substantial alteration of most feldspars to sericite is observed, further contributing to the rock's mineralogical composition. Despite the relatively low cementation, the clay

matrix between grains plays a significant role in shaping the overall characteristics of this rock. The detailed examination of sample TBS-1 enhances our understanding of sedimentary dynamics, transportation processes, and the influence of source area geology on the reservoir's physical and chemical properties.

Figure 5. (a) Photograph of a non-polished slide of the plug of the sandstone TBS-1 and its characteristic texture under the stereomicroscope. (b)-(c)-(d) Photomicrographs in plane-polarized light and crossed-polarized light of the analyzed sandstone.
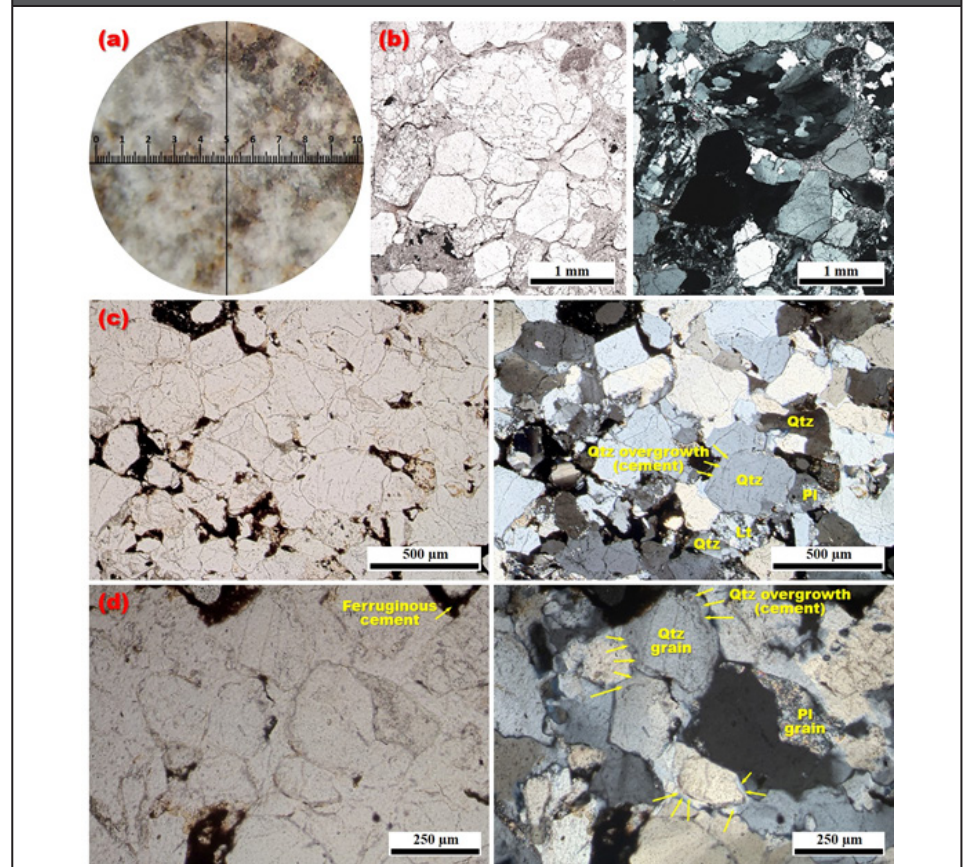
Samples PIC-1 (Figure 6) and PIC-2 (Figure 7) are classified texturally as sandstones and compositionally as fine to medium-grained sublitarenite and subakose, respectively, with grains of subangular shape, with low sphericity. These rocks show good selection and the contacts between particles can be concave-convex, point and sutured, which is manifested mainly in the grains of mainly monocrystalline quartz and potassium feldspar. These rocks present a small amount of matrix and cement, with the presence

of quartz, clays and iron oxides, muscovite and zircon mainly as accessory minerals and, locally, lithic fragments. They show a fine-grained matrix, which indicates that it is essentially clay minerals. In sample PIC-1, most of the rigid grains are rounded to sub-rounded with a good selection, which come from a more continental origin and may be alluvial deposits or abyssal plains. The large grains are composed of quartz, potassium feldspar, plagioclase, biotite, chlorite and rock fragments. Feldspars show alteration to sericite. In sample PIC-2, most of the rigid grains are rounded to sub-rounded with a good selection, which come from different alluvial environments. The large grains are composed of quartz, potassium feldspar and a small amount of plagioclase. Quartz sometimes exhibits wavy extinction due to deformation. Most of the feldspar shows strong alteration to sericite.

Figure 6. (a) Photograph of a non-polished slide of the plug of the sandstone PIC-1 and its characteristic texture under the stereomicroscope. (b)-(c)-(d) Photomicrographs in plane-polarized light and crossed-polarized light of the analyzed sandstone. Note the concave-convex, point and sutured between quartz (Qtz) and orthoclase (Or) indicated by yellow arrows.

Figure 7. (a) Photograph of a non-polished slide of the plug of the sandstone PIC-2 and its characteristic texture under the stereomicroscope. (b)-(c)-(d) Photomicrographs in plane-polarized light and crossed-polarized light of the analyzed sandstone. Note the concave-convex, point and sutured between quartz (Qtz) and orthoclase (Or) indicated by yellow arrows.
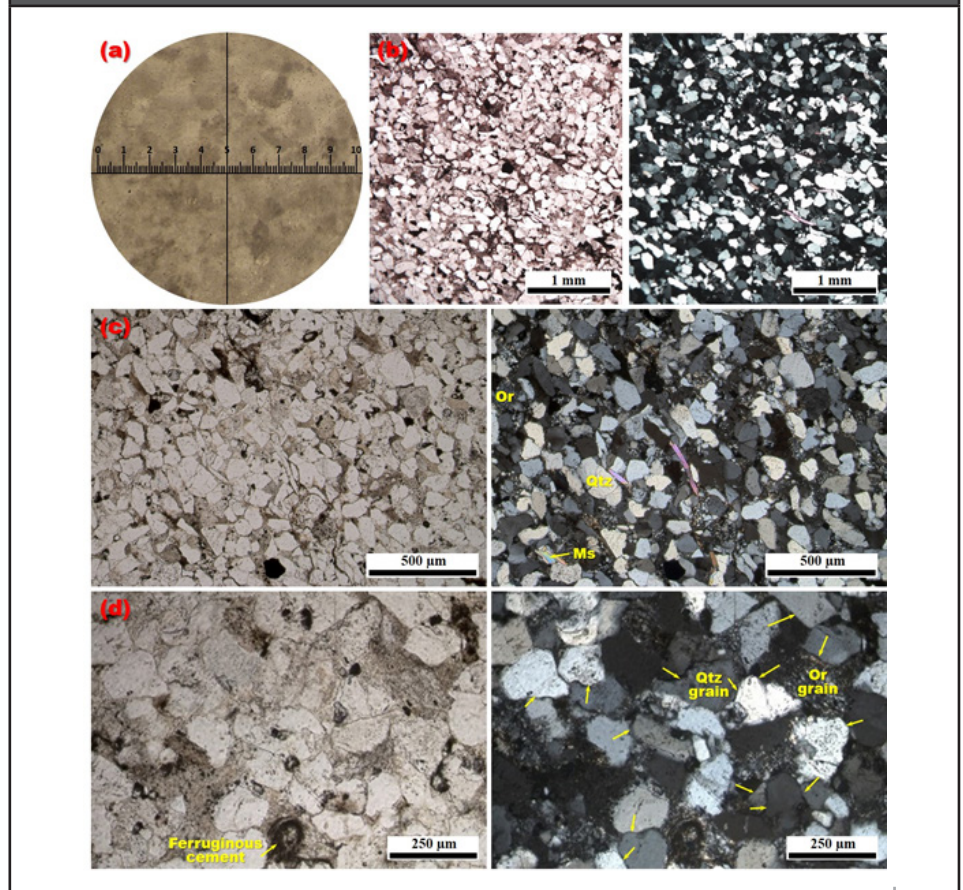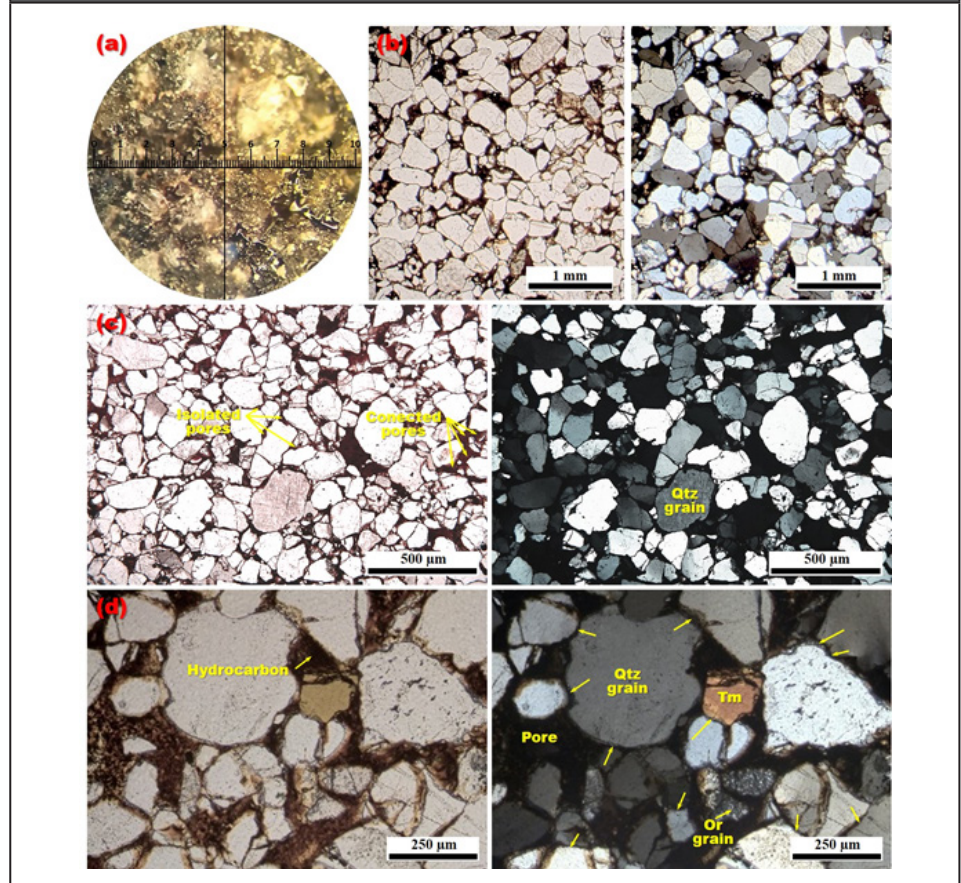
3.3. X-ray diffraction analysis

The X-ray diffraction patterns depicted in Figures 8-12 provide a comprehensive insight into the mineralogical composition of the analyzed sandstones. Notably, all quartz and a corundum standard (α-phase) are highlighted for quantitative analysis. Quartz signals at 21.4 of 2θ and plagioclase feldspars at 23.5 2θ are general observations across the samples. However, a more nuanced exploration of the clay minerals, ranging between 3.5 and 34 degrees of 2θ, reveals intricate details. In the case of samples TIB-1 (Figure 8a) and ARC-1 (Figure 9a), the detection of micas signals suggests potential illite presence at 8.8 2θ, with a corresponding basal spacing (d) of 9.99 Å. Furthermore, ARC-1 exhibits signals attributed to kaolinite and chlorite at 12.5 and 6.2 2θ, respectively.

While these signals provide initial insights, a more in-depth analysis involving diffraction and treatment of the clay fraction is imperative to precisely identify mineral species associated with each signal. The presence of micas and kaolinite signals is pronounced on to samples LSA-1 (Figure 10a) and TBS-1 (Figure 11a). Additionally, LSA-1 raises the possibility of smectite, vermiculite, and chlorite presence, particularly indicated by the peak signal at 6.2 2θ. Meanwhile, in samples PIC-1 (Figure 12a) and PIC-2 (Figure 12d), the dominance of kaolinite signals is evident, with potential overlap from chlorite signals within the candite group. It's noteworthy that no signals indicating interstratification have been identified. This detailed exploration reveals the diverse mineralogical composition of the samples, encompassing varying amounts of micas, kaolinite, chlorite, vermiculite or smectite, albite, and quartz. These nuanced mineralogical insights will be instrumental in unraveling the intricate petrophysical properties and understanding the influence of clay minerals on the overall behavior of the sandstones.
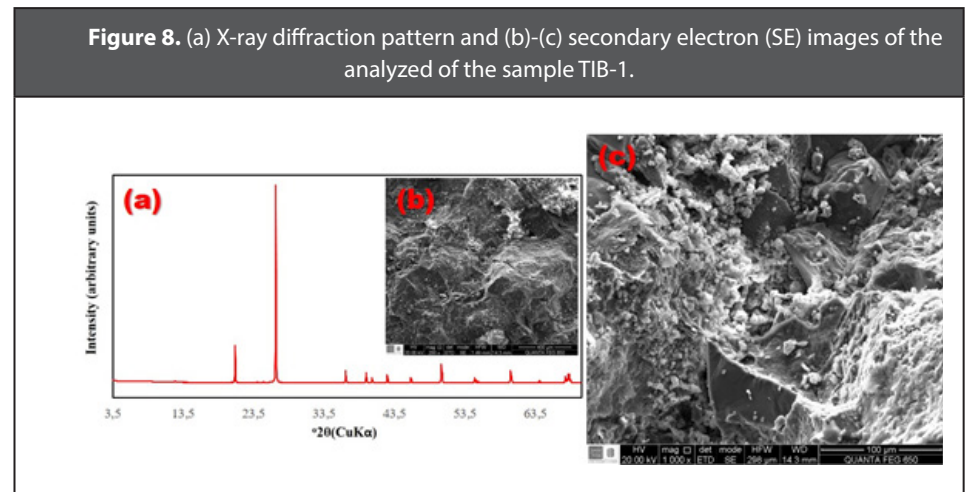

Figure 8. (a) X-ray diffraction pattern and (b)-(c) secondary electron (SE) images of the analyzed of the sample TIB-1.

Figure 9. (a) X-ray diffraction pattern and (b)-(c) secondary electron (SE) images of the analyzed of the sample ARC-1.
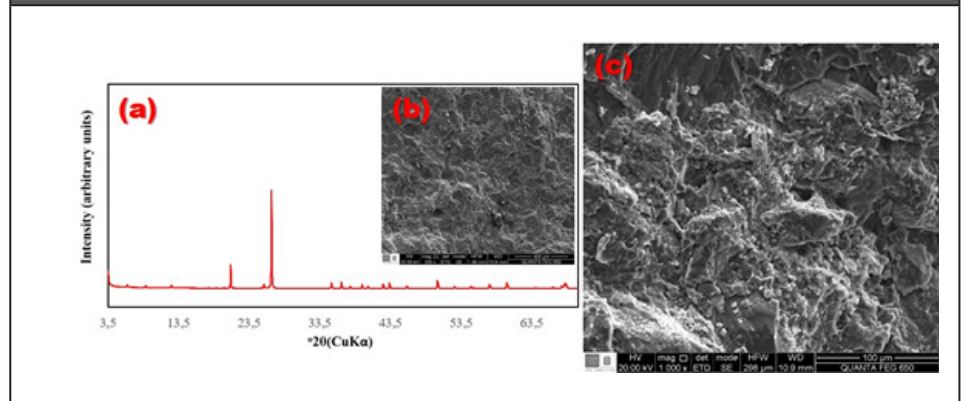

Figure 10. (a) X-ray diffraction pattern and (b)-(c) secondary electron (SE) images of the analyzed of the sample TBS-1.
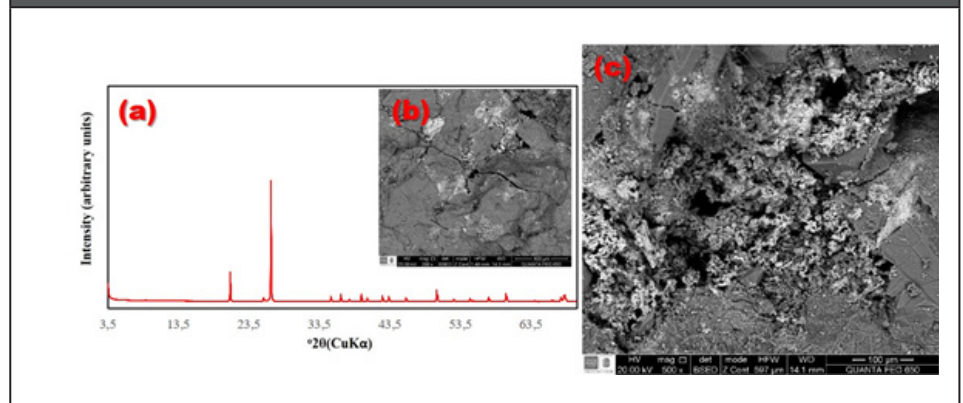

Figure 11. (a) X-ray diffraction pattern and (b)-(c) secondary electron (SE) images of the analyzed of the sample LSA-1.
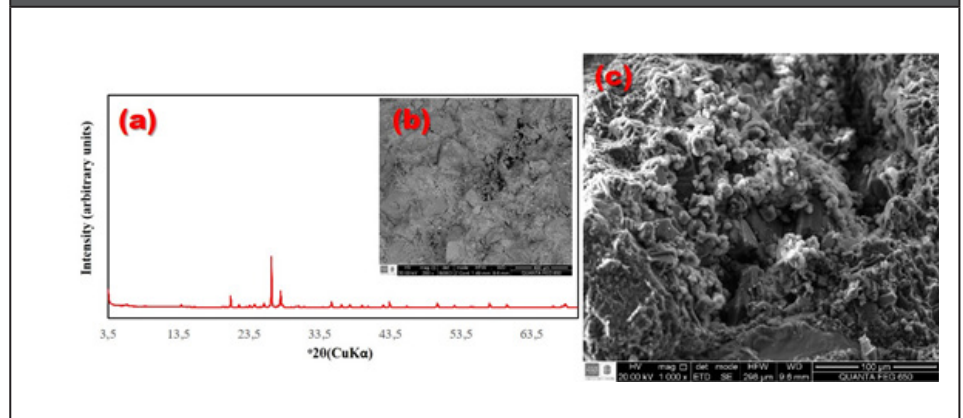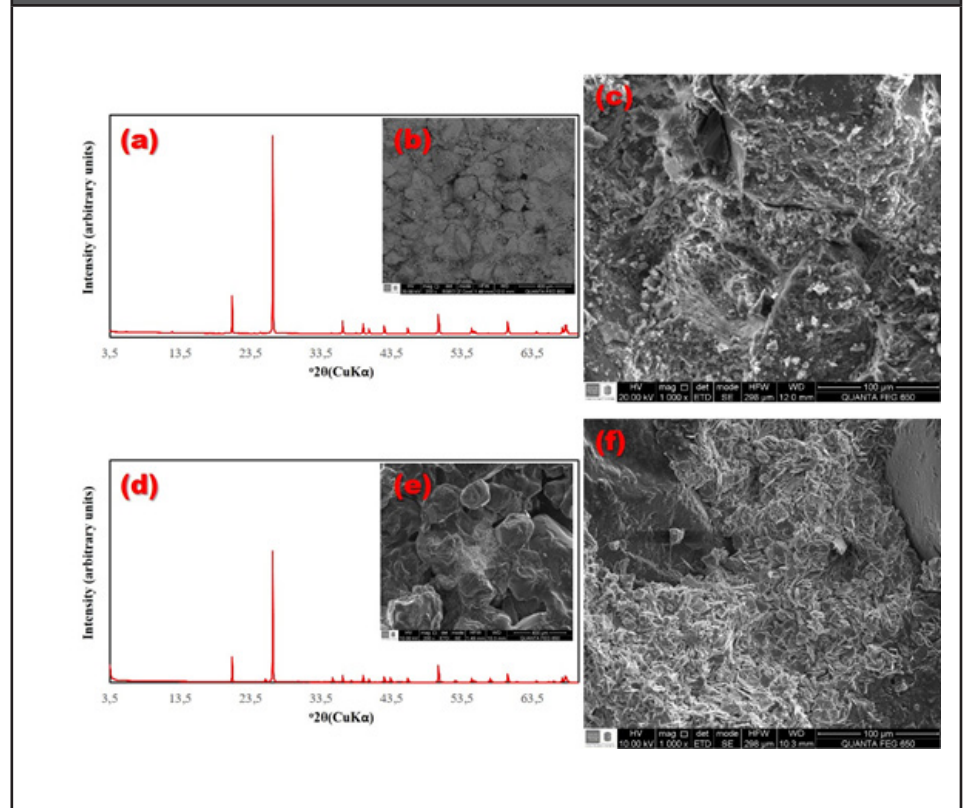
Figure 12. (a) X-ray diffraction pattern and (b)-(c) secondary electron (SE) images of the analyzed of the sample PIC-1. (d) X-ray diffraction pattern and (e)-(f) secondary electron (SE) images of the analyzed of the sample PIC-2.

3.4. Scanning electron microscopy

The SEM analysis provides a fascinating glimpse into the intricate microstructures of the investigated sandstones, allowing us to peer into the pores, identify minute minerals, and observe their distribution within these spaces. Figures 8-12 show the microstructure of three sandstones with varying grain sizes, each revealing unique characteristics. Sample TIB-1 (Figures 8b-8c) exhibits a dense structure with clear boundaries, numerous pores, a moderate degree of cementation, and an abundance of clay minerals. Quartz is closely surrounded by clay minerals, emphasizing the intricate interplay within the matrix. The sample ARC-1 (Figures 9b-9c) shows a very dense structure with fuzzy boundaries, fewer pores, high cementation, and an abundance of clay minerals is observed. Quartz is closely surrounded by

clay minerals. Sample LSA-1 (Figures 10b-10c) presents a coarse-grained sandstone with a considerable matrix, where plagioclase has undergone alteration to sericite. Clay minerals and microcrystalline quartz fill the pores, while authigenic quartz cement is evident as a pore-occluding mineral in deeply buried sandstone. Notably, some reservoirs at depths exceeding 2500 m may contain more porosity than predicted by existing conceptual models of quartz cementation (French et al., 2012). In the case of sample TBS-1 (Figures 11b-11c), authigenic clay minerals, particularly kaolinite, present a visually striking appearance. At a smaller scale, micrographs reveal authigenic kaolinite in a pseudo-vermicular form and goethite in concentric chopstick-like structures of 2 μm. The sample PIC-1 (Figures 12b-12c) is characterized by a coarse-grained structure with a higher matrix content than PIC-2 (Figures 12d-12e). Pores in PIC-1 contain kaolinite particles, microcrystalline quartz, and illite pore bridging. While kaolinite contributes to microporosity development without significant damage to the formation, pore-bridging illite adversely impacts permeability, causing serious formation damage (Kantorowicz, 1990). Finally, PIC-2 displays a loose structure with clear boundaries, numerous pores, minimal cementation, few clay minerals, and minerals Si surrounded sparsely by clay minerals. This comprehensive SEM analysis unveils the diverse microstructural intricacies inherent in each sandstone sample.

3.5. Basic petrophysical properties

Understanding the reservoir quality of sandstones necessitates a nuanced examination of their distinct petrophysical parameters, as emphasized by Shogenov et al. (2015). It is crucial to recognize that the pore space within these sandstones intricately governs their fundamental petrophysical properties, primarily porosity and permeability. Table 1 provides a comprehensive overview of the key petrophysical data extracted from the analyzed sandstones, revealing a diverse range of values across various parameters. The Klinkenberg permeability, spanning from 0.057 to 1383.281 mD, and air permeability, ranging between 0.142 and 1429.272 mD, showcase the

considerable variability in the ability of these sandstones to transmit fluids. The slip factor, b, demonstrates a noteworthy range from 0.499 to 67.663 psi, reflecting the resistance encountered by fluids during flow through porous media. Inertial coefficients, α (17.760-1.494.722 μm) and β (3.965.184-122.729.00 ft^{-1}), offer insights into the inertia-related parameters influencing fluid flow behavior within the sandstone matrix. Exploring the volumetric aspects, the real pore volume spans from 34.785 to 59.859 cm^3, underscoring the variability in the available pore spaces within these sandstone samples. Porosity, a fundamental property, ranges from 1.812 to 20.649%, providing a quantitative measure of the void spaces relative to the total volume of the rock. The grain volume, representing the total space occupied by solid grains, exhibits variations from 31.801 to 58.774 cm^3. Concurrently, grain density fluctuates within a range of 2.583 to 2.704 g/cm^3, emphasizing the density variations among the solid constituents of the sandstones. This comprehensive exploration of petrophysical parameters lays the foundation for a nuanced understanding of the diverse reservoir qualities exhibited by the analyzed sandstones. The intricate interplay between porosity and permeability, along with the variations in volumetric properties, contributes to the unique characterization of each sandstone sample.

Table 1. Basic petrophysical properties of the analyzed sandstones (adapted and modified after Paba-Santiago, 2018).

Parameter	TIB-1	ARC-1	LSA-1	TBS-1	PIC-1	PIC-2
Length (mm)	39.90	52.10	30.27	44.48	51.79	34.96
Diameter (mm)	38.32	38.26	38.28	44.48	38.18	38.23
Weight (g)	119.18	157.18	86.14	119.04	131.29	82.14
Confining pressure (psi)	400	400	400	400	400	400
Klinkemberg permeability (mD)	0.057	0.002	1.839	25.788	17.603	1383.281
Air permeability (mD)	0.142	0.009	2.408	29.220	19.888	1429.272
Grain volume (cm^3)	44.081	58.774	32.902	44.670	49.403	31.801
Pore volume (cm^3)	1.878	1.085	1.883	6.109	9.798	8.275
Grain density (g/cm^3)	2.704	2.674	2.618	2.665	2.658	2.583
Porosity (%)	4.085	1.812	5.414	12.031	16.550	20.649
slip factor, b (psi)	22.243	67.663	4.642	1.997	1.947	0.499
α (μm)	804.067	271.915	730.836	1.494.722	240.321	17.760
β (ft^{-1})	4.341.501	51.069.290	122.729.900	17.900.850	4.216.193	3.965.184

In the context of reservoir evaluation, Tiab and Donaldson (2012) delineate the criteria for optimal porosity and permeability conducive to efficient oil and gas extraction. According to their findings, the threshold for a "good" reservoir entails a porosity falling within the range of 15–20% and permeability between 50–250 mD. This benchmark serves as a reference point for identifying reservoirs with the potential for robust hydrocarbon production. Building upon this foundation, Shogenov et al. (2015) have undertaken a nuanced categorization of reservoir sandstones, introducing a classification system encompassing four distinct groups and eight classes, as outlined in Table 2. The demarcation between these groups is established based on specific permeability thresholds: 300, 100, 10, and 1 mD. Each group, in turn, is further subdivided into two classes, delineated by varying porosity levels. This systematic classification not only refines the understanding of reservoir quality but also facilitates a more detailed and targeted assessment of the diverse characteristics inherent in reservoir sandstones. By incorporating these classifications into the broader context of reservoir characterization, researchers and industry professionals gain a more nuanced perspective on the intricate interplay between porosity and permeability. This multifaceted approach enhances the ability to identify and categorize reservoirs, providing valuable insights into their potential for effective hydrocarbon recovery and contributing to the optimization of exploration and production strategies.

Table 2. Classification of reservoir rocks according to permeability and porosity (adapted and modified from Shogenov et al., 2015).

Group	Application for CGS	Class	Reservoir quality	K (mD)	Φ (%)
1	Very appropriate	I	High-1	> 300	> 20
		II	High-2		9-20
2	Appropriate	III	Good	100-300	> 18
		IV	Moderate		9-18
3	Cautionary	V	Cautionary-1	10-100	18-23
		VI	Cautionary-2		7-18
4	Not appropriate	VII	Low	1-10	7-18
		VIII	Very low	< 1	< 18

-The analyzed reservoir rocks (Figure 13) belong to two groups and four classes of this classification scheme. Samples TIB-1 and ARC-1 show K and Φ in the ranges of 0.009-0.142 mD and 1.81-4.09 %, respectively. They represent the group 4 and the class VIII, which are not appropriate for CGS and are very low-quality reservoirs. Sample LSA-1, showing K of 2.400 mD and Φ of 5.55 %, represents the group 4 with characteristics between classes VII and VIII, which is not appropriate for CGS and is a low to very low-quality reservoir. Samples TBS-1 and PIC-1 show K and Φ in the ranges of 19.880-29.220 mD and 12.19-16.68 %, respectively. They represent the group 3 and the class VI, which are cautionary for CGS and are cautionary-2 quality reservoirs. Sample PIC-2, showing K of 14.290 mD and Φ of 20.75 %, represents the group 3 and the class V, which is cautionary for CGS and is a cautionary-1 quality reservoir. The analyzed sandstones have low porosity, although high permeability, with the last of them dramatically affected by grain size (800mD at very coarse-grained sandstone and 90mD at fine-grained sandstone both at 10% porosity). They also report that these sandstones have very low vertical permeability, compared to horizontal (Kv/Kh = 0.1 or less, dependent on formation permeability). The reservoir quality of rocks decreases with increasing depth because of rock compaction, rising temperature, conformation of grains and increasing quartz cementation of sandstone (e.g., Sliaupa et al., 2001; Shogenov et al., 2015; Fan et al., 2019). Our study confirms these results, considering that the analyzed sedimentary rocks are highly mature sandstones, strongly compacted and cemented with little early infiltrated clay minerals, with very small intergranular pore space, which according to Stück et al. (2013b) can be attributed to compaction and cementation. The degree of quartz cementation represents one of the diagenetic processes having most influence on reservoir properties and quality (Molenaar et al., 2007). However, compaction is believed to be the most important parameter influencing primary porosity loss during diagenesis (Schmidt, et al., 1997). The analyzed reservoir rocks belong to two groups and four classes of the classification scheme proposed by Shogenov et al. (2015), with K and Φ in the ranges of 0.009-29.220 mD and 1.88-20.75 %, respectively. Porosity and permeability are related to different properties of pore space geometry. Results reveal two main types of sandstones: (1) very

low values (K = 0.009-0.570 mD and Φ = 1.880-5.020 %) for highly cemented sandstones of the Tibet (TIB-1) and Arcabuco (ARC-1) formations due to a high share of carbonate cement, and (2) moderate values (K = 19.880-29.220 mD and Φ = 12.19-16.68 %) for moderately cemented sandstones of the Tibasosa (TBS-1) and Picacho (PIC-1) formations. The porosity percentages of sandstones from the Arcabuco (ARC-1) and Picacho (PIC-2) formations are the lowest (1.88 %) and highest (20.75 %), respectively. The first one represents a sandstone not appropriate for CGS, which is very low-quality reservoir, whereas the second one represents a sandstone cautionary for CGS, which is a cautionary-1 quality reservoir. This strong difference is explained by compaction and secondary quartz cementation. However, the reservoir quality of the analyzed sandstones is strongly affected by a set of petrophysical, chemical, mineralogical and microstructural parameters.

Figure 13. Gas permeability versus porosity of the measured reservoir sandstones in the Eastern Cordillera (PIC-1, PIC-2, TBS-1, ARC-1, TIB-1) and Middle Magdalena Valley (LSA-1) basins, showing the eight reservoir quality classes suggested by Shogenov et al. (2015).
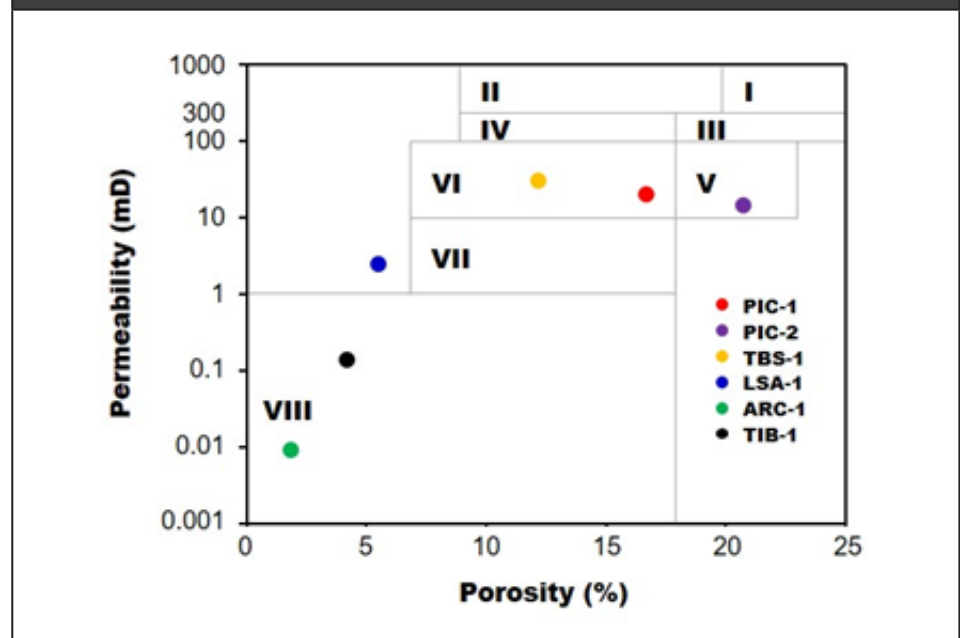
## 4. Effect of clay minerals on porosity and permeability

The discussion on the impact of clay minerals on the petrophysical properties of the analyzed sandstones reveals a complex interplay of factors influencing porosity and permeability. As highlighted by Shogenov et al. (2015), the petrophysical properties (porosity and permeability) of a reservoir are the result of grain size, sorting and pore structure, cementation, diagenetic alteration, burial depth and compaction, tectonic and geothermal conditions and facial variation, which can be associated to the major minerals (quartz and feldspar, clays, and carbonate). However, we make emphasize on the role of clay minerals on the porosity and permeability of the analyzed rocks. The petrophysical properties control the flow and storage of fluids in sedimentary rocks (Šperl and Trčková, 2008). The influence of clay minerals on these properties is well-documented in the literature, with several studies (Morris and Shepperd, 1982; Šperl and Trčková, 2008; Shogenov et al., 2015; Li et al., 2016) emphasizing the significance of factors such as pore-size distribution, clay particle sizes, distribution within the pore space, and clay composition. The interpretation of porosity and permeability results (Figure 13) in relation to the presence and percentage of clay minerals can provide important insights into the petrophysical properties of rocks. In examining the relationship between rigid grains (quartz and feldspar) and porosity, this study aimed to gain insights into the petrophysical properties of rocks. Generally, clay minerals are associated with lower porosity as their particles fill the pore spaces between sand grains, reducing total porosity. The Arcabuco Formation (ARC-1) stands out with the lowest porosity values, indicating a potentially higher proportion of clay minerals contributing to decreased porosity. On the other hand, the presence of clay minerals can obstruct porous channels and reduce pore connectivity, negatively impacting permeability. Conversely, sandstones from the Picacho (PIC-1 and PIC-2) and Tibasosa (TBS-1) formations show higher permeability values, suggesting a lower presence of clay minerals or a favorable distribution allowing better pore connectivity. Variability in results between formations may indicate differences in mineral composition, including the quantity and type of clay minerals present. However, a

more detailed analysis of clay content in each sample can provide a more accurate understanding of how the presence and percentage of clay minerals affect petrophysical properties. The petrophysical properties are subject to multiple diagenetic processes. The findings of Zhao et al. (2015) challenge a straightforward link between quartz content and porosity, attributing it to silica precipitation phenomena. A common phenomenon is visible in sandstones, the dissolution of rigid grains of feldspar, particularly in tight sandstones, which can cause porosity at nanometer scale. Regarding the influence of clay minerals on porosity and permeability, it is important to establish how they affect the pores and pore throats. Microstructural analysis, as depicted in Figures 14-15, further illustrates the intricate relationship between rigid grains of quartz and/or feldspar and clay minerals. The formation of clay aggregates and the subsequent infilling of interparticle pores contribute to a significant loss in porosity by impeding fluid flow. The type and volume of clay minerals occupying pores, such as illite, kaolinite, vermiculite, and chlorite, play a crucial role in determining the overall petrophysical properties. However, microcrystalline quartz, goethite, and feldspar dissolution can also influence the petrophysical properties of the investigated sandstones.

Examining the impact of specific clay minerals on porosity and permeability, illite emerges as a predominant clay mineral, especially in tight sandstones with significant clay matrix content. In contrast, sandstones with lower clay matrix content, such as PIC-1 (Figure 14a) and PIC-2 (Figure 14b), exhibit greater porosity, supporting the notion of a negative correlation between clay matrix and porosity. This aligns with findings from previous works (e.g., Zhao et al., 2016; Jianfeng et al., 2013; Storvoll et al., 2002), which suggest a negative relationship between illite and interstratified I/S with the porosity and permeability. The sample PIC-1 shows a clay matrix in most of the sample, good primary porosity, secondary porosity associated to agglomerates of clay minerals with microporosity. Among the clay agglomerates, there are large pores of interparticle and occasionally intraparticle type. This example can illustrate a typical dissolution of matrix and cement in the rock. The sample PIC-2, although it is impregnated with oil, highlights its scarce clay matrix

and cementation of the grains (there are no grains in solution or clay minerals infilling between the grains). It shows intergranular primary and secondary pores, and microporosity in the discrete packages of kaolinite, which is sometimes disoriented and this further reduces the microporous space between clay minerals, which is a habitual behavior of this clay mineral. This mineral, like smectite and chlorite, can occur as cementitious materials, but they are less documented than other more characteristic minerals (Burley and Worden, 2003). The authigenic origin of clay minerals, such as kaolinite and goethite, introduces another layer of complexity. The sample TIB-1 (Figure 14c) shows several types of pores and microporosity between aggregates of clay minerals (less than 5 μm), which are not completely infilling between the pores but they highlight porous spaces up to 50 μm. This is characteristic of kaolinites as can be seen in the analyzed sample as can be seen in this sample, which is in discrete particles. We also highlight the presence of illite and traces of iron and titanium oxides. Illite develops aggregates infilling pores.

Figure 14. Pore morphology of the analyzed TIB-1, ARC-1 and LSA-1 sandstones.
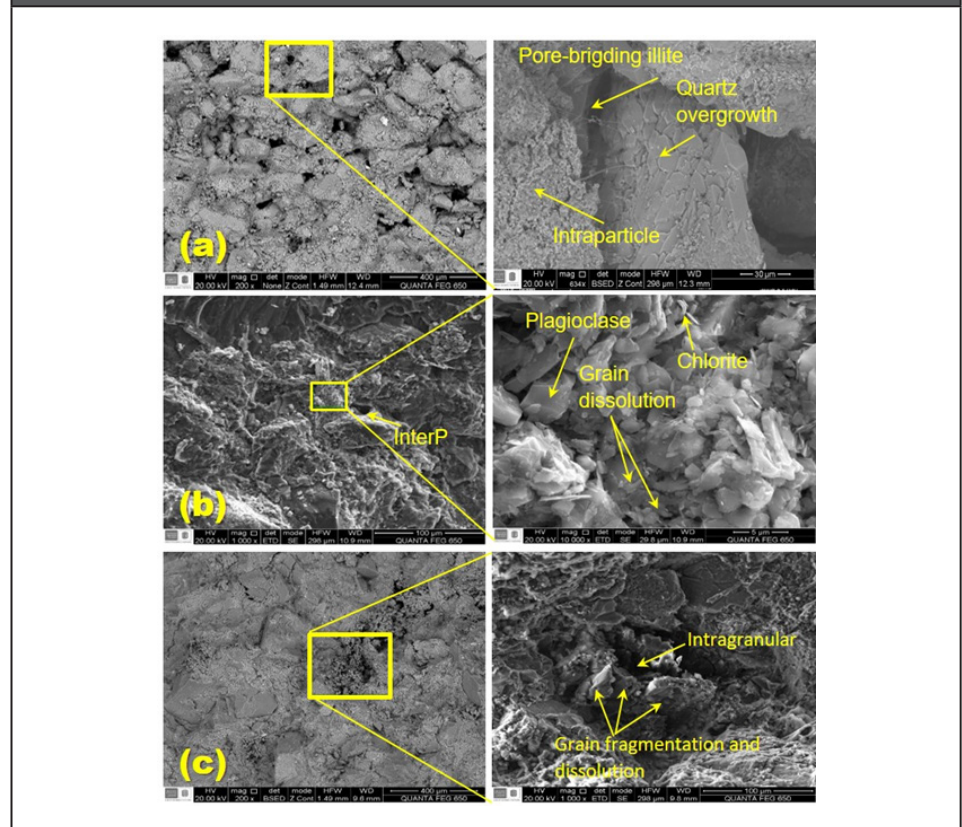
The sample TBS-1 (Figure 15a) is characterized by the occurrence of authigenic clay minerals. The discrete packages of kaolinite are well ordered and spaced, where their porosity is even greater than the microporosity. This sample is quite clayish and presents fractured grains and clay minerals within those spaces, but also presents microporosity between the spaces of clay minerals and goethite, which allows pores to appear between the clay aggregates, due to its way of coating the walls of the pores. The sample TBS-1 shows less porosity and higher permeability than the PIC-1 sample, which is due to the presence of microfractures of rigid grains, the predominance of authigenic clay, the occurrence of goethite contributes to protect the porosity, while the presence of pore-bridging illite that reduces permeability and does not affect the porosity in PIC-1. Therefore, the permeability as a filtering capacity of the clay minerals suffers the funnel effect in the poral throats that are mainly affected by a morphology that involves many walls of the interparticle spaces, in such a way that a pore-bridging illite could have catastrophic effects for an oil reservoir. The presence of kaolinite correlates positively with porosity, especially in samples with greater porosity and good permeability (PIC-1, PIC-2, and TBS-1). These authigenic minerals exhibit well-ordered structures and contribute significantly to microporosity. The sample ARC-1 (Figure 15b) is characterized by the occurrence of clays dominated pores, that is, there are particles of clay minerals infilling between the pores, which is also helped by the abundant matrix that generates a very prominent microporosity and, therefore, a very low porosity and permeability. The sample LSA-1 (Figure 15c) exhibits a pore-filling due to a large amount of contribution of the altered and infilling between the pore's feldspars, which may indicate that the sample was affected by dissolution of rigid grains and seriticitization of feldspar. In general, this sample presents aggregates of clay minerals with porosity, grain dissolution and interparticle and intraparticle porosity. According to Zhao et al. (2015), porosity is closely related to reservoir storage capacity, while permeability controls the filtration process. Furthermore, the origin of clay minerals should be considered, distinguishing between detrital clays blocking interparticle pores during compaction in the early diagenesis and authigenic clay blocking pores in the middle and final stages of diagenesis. Understanding the sedimentation,

transport, and compaction processes of reservoir rocks is essential for interpreting porosity and permeability of great importance in the hydrocarbon industry. On the other hand, it is important to consider the geometry and volume of occupation of clay minerals in the pores. Morris and Shepperd (1982) divided the clay particles of the sandstones into three general types: discrete particles, pore-lining and pore-bridging, which can be distinguished in the analyzed samples and described below. The analyzed sandstones show discrete particles, pore-bridging and a type of discrete particles called pore-filling, characteristic of clay minerals such as illite and kaolinite, quartz, carbonates and micas (Wolela, 2006). Regarding how porous spaces occupy and pores affect the clay minerals and based on Yao et al. (2013), the analyzed samples show pores that have been classified into four types: residual interparticle (interP) pores, grain dissolution pores, clay dominated pores and microfractures, which is of great importance in the exploration of gas associated to tight sandstone, tight oil, shale oil, and coal bed methane or other unconventional oil and gas resources.

Figure 15. Pore morphology of the analyzed TBS-1, PIC-1 and PIC-2 sandstones.
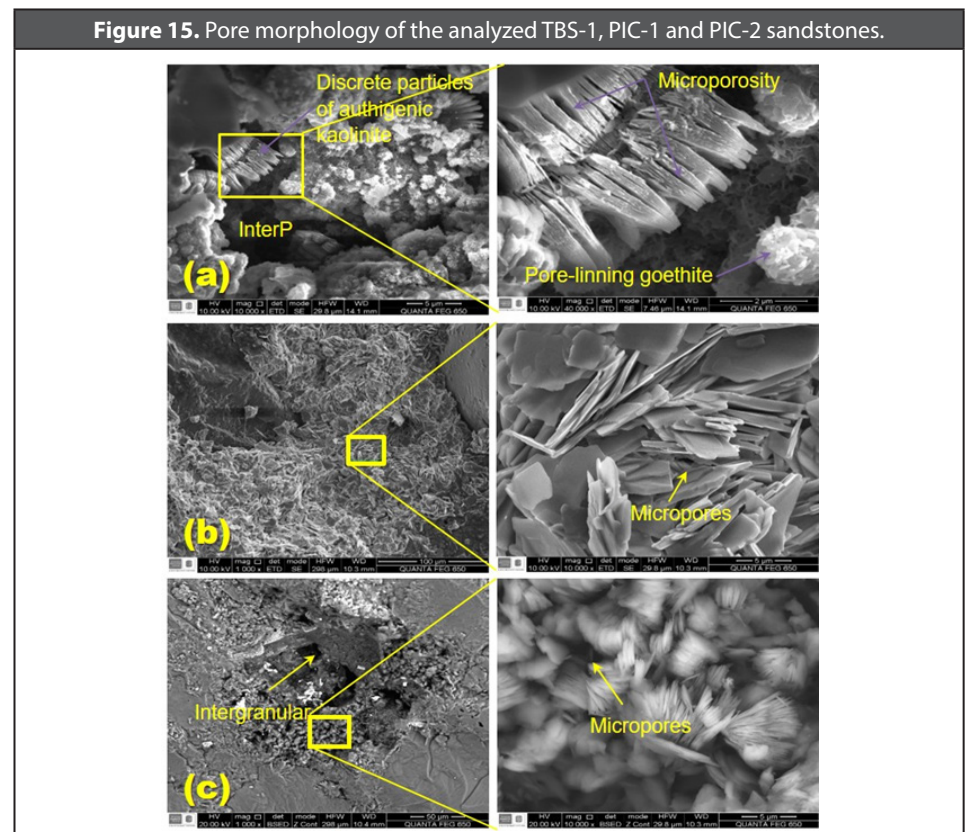
The investigated sandstones in the context of hydrocarbon exploration and production provides valuable information about their potential as reservoirs and their future in terms of extraction. The Arcabuco Formation (ARC-1), with the lowest porosity values, could indicate a lower capacity to host fluids, potentially affecting hydrocarbon storage and production. Low porosity may require specialized production strategies, such as well stimulation, to enhance hydrocarbon recovery. Sandstones from the Picacho (PIC-1 and PIC-2) and Tibasosa (TBS-1) formations, with higher permeability values, suggest a better ability for fluid flow through the formation. Higher permeability can be favorable for hydrocarbon extraction, improving fluid mobility and increasing production efficiency. A more detailed analysis of clay content in each formation is essential to understand its specific impact on petrophysics and the challenges it may pose in terms of production. The presence of clays can influence well stability, the effectiveness of stimulation, and other extraction-related aspects. The reservoirs within the Eastern Cordillera and Middle Magdalena Valley basins exhibit characteristics of tight, complex formations, posing challenges in predicting intricate accumulation mechanisms. Furthermore, this oil basin demonstrates medium maturity, significant diagenesis, fine to medium-sized rock particles, effective calibration, high cement content, and considerable heterogeneity. It is crucial to highlight the nuanced interplay between clay minerals and petrophysical properties, underscoring the necessity for a thorough comprehension of mineralogical compositions, diagenetic processes, and pore structures. This comprehensive understanding is essential to improve reservoir characterization and optimize exploration and production strategies in the face of the complexities posed by these geological settings.

5. Conclusions

Macroscopic analysis reveals variations in weathering conditions, compactness, grain size, sphericity, roundness, color, and mineral composition among the sandstone samples. Detrital texture provides

insights into endurance, porosity, and permeability, while mineral composition influences reservoir quality factors like cementation and porosity. Transmitted light microscopy emerges as a valuable method, enabling a nuanced understanding of detrital components' relationships and their impact on physical and chemical reservoir properties.

XRD patterns unveil the diverse mineralogical composition, including quartz, plagioclase feldspars, illite, kaolinite, chlorite, vermiculite, and others. Different sandstone samples exhibit varying clay mineral signals, contributing to the complex petrophysical properties observed.

SEM analysis provides detailed insights into the microstructures of sandstones, emphasizing variations in pore spaces, cementation, and the presence of authigenic clay minerals. Microstructural intricacies contribute to the understanding of how clay minerals impact porosity and permeability, influencing reservoir quality.

Petrophysical parameters, including porosity, permeability, and volumetric properties, showcase considerable variability among the sandstone samples. Application of established reservoir quality criteria and classifications categorizes the samples into distinct groups and classes, offering insights into their hydrocarbon production potential.

The intricate relationship between clay minerals and petrophysical properties is highlighted, emphasizing the negative correlation between clay matrix and porosity. Microstructural analysis reveals the impact of specific clay minerals like illite and kaolinite on pore spaces, influencing reservoir storage capacity and filtration processes.

The study underscores the importance of a holistic understanding of mineralogical compositions, diagenetic processes, and pore structures for effective reservoir characterization in challenging geological settings. Recognizing the complex interplay of factors influencing detrital texture and petrophysical properties is crucial for optimizing exploration and production strategies in diverse reservoirs.

6. Acknowledgements

7. References

Aguilera, R., Sotelo, V., Burgos, C., Arce, C., Gómez, C., Mojica, J., Castillo, H., Jiménez, D. & Osorno, J. (2010). Organic Geochemistry Atlas of Colombia. *Earth Sciences Research Journal, Special Edition*, 14, 1-174.

Al-Kharra'a, H.S., Wolf, K.H.A.A., AlQuraishi, A.A., Mahmoud, M.A., Deshenenkov, I., AlDuhailan, M.A., Alarifi, S.A., AlQahtani, N.B., Kwak, H.T. & Zitha, P.L.J. (2023). Impact of clay mineralogy on the petrophysical properties of tight sandstones. *Geoenergy Science and Engineering*, 227, Article 211883. https://doi.org/10.1016/j.geoen.2023.211883

Anovitz, L.M. & Cole, D.R. (2015). Characterization and analysis of porosity and pore structures. *Reviews in Mineralogy and Geochemistry*, 80(1), 61–164. https://doi.org/10.2138/rmg.2015.80.04

Bera, B., Mitra, S.K. & Vick, D. (2011). Understanding the microstructure of Berea Sandstone by the simultaneous use of micro-computed tomography (micro-CT) and focused ion beam-scanning electron microscopy (FIB-SEM). *Micron*, 42(5), 412-418. https://doi.org/10.1016/j.micron.2010.12.002

Burley, S.D. & Worden, R.H. (2003). Sandstone Diagenesis: The Evolution of Sand to Stone. In: Sandstone Diagenesis, Recent and Ancient (Burley, S.D., Worden, R.H., Eds.), *Blackwell Publishing: Malden, MA, USA*, pp. 1–44.

Caballero, V.M., Parra, M. & Mora, A.R. (2010). Levantamiento de la Cordillera Oriental de Colombia durante el Eoceno Tardío - Oligoceno Temprano: Proveniencia sedimentaria en el Sinclinal de Nuevo Mundo, Cuenca Valle Medio del Magdalena. *Boletín de Geología*, 32(1), 45-77.

Campos, R., Barrios, I. & Lillo, J. (2015). Experimental CO2 injection: Study of physical changes in sandstone porous media using Hg porosimetry and 3D pore network models. *Energy Reports*, 1, 71-79. https://doi.org/10.1016/j.egyr.2015.01.004

Combes, R., Robin, M., Blavier, G., Aïdan, A. & Degrève, F. (1998). Visualization of imbibition in porous media by environmental scanning electron microscopy: application to reservoir rocks. *Journal of Petroleum Science and Engineering*, 20(3–4), 133-139. https://doi.org/10.1016/S0920-4105(98)00012-6

Cooper, M.A., Addison, F.T., Alvarez, R., Coral, M., Graham, R.H., Hayward, A.B., Howe, S., Martinez, J., Naar, J., Penas, R., Pulham, A.J. & Taborda, A. (1995). Basin Development and Tectonic History of the Llanos Basin, Eastern Cordillera, and Middle Magdalena Valley, Colombia. *American Association of Petroleum Geologists Bulletin*, 79(10), 1421–1442. https://doi.org/10.1306/7834D9F4-1721-11D7-8645000102C1865D

Desbois, G., Urai, J.L., Kukla, P.A., Konstanty, J. & Baerle, C. (2011). High-resolution 3D fabric and porosity model in a tight gas sandstone reservoir: A new approach to investigate microstructures from mm- to nm-scale combining argon beam cross-sectioning and SEM imaging. *Journal of Petroleum Science and Engineering*, 78(2), 243-257. https://doi.org/10.1016/j.petrol.2011.06.004

Desbois, G., Urai, J.L., Hemes, S., Schröppel, B., Schwarz, J.-O., Mac, M. & Weiel, D. (2016). Multi-scale analysis of porosity in diagenetically altered reservoir sandstone from the Permian Rotliegend (Germany). *Journal of Petroleum Science and Engineering*, 140, 128-148. https://doi.org/10.1016/j.petrol.2016.01.019

Fan, A., Yang, R., Lenhardt, N., Wang, M., Han, Z., Li, J., Li, Y. & Zhao, Z. (2019). Cementation and porosity evolution of tight sandstone reservoirs in the Permian Sulige gas field, Ordos Basin (central China). *Marine and Petroleum Geology*, 103, 276-293. https://doi.org/10.1016/j.marpetgeo.2019.02.010

French, M.W., Worden, R.H., Mariani, E., Larese, R.E., Mueller, R.R. & Kliewer, C.E. (2012). Microcrystalline quartz generation and the preservation of porosity in sandstones; evidence from the Upper Cretaceous of the Subhercynian Basin, Germany. *Journal of Sedimentary Research*, 82(6), 422–434. https://doi.org/10.2110/jsr.2012.39

García, M., Mier, R., Cruz, L.E. & Vásquez, M. (2009). Evaluación del potencial hidrocarburífero de las cuencas colombianas. Contrato Interadministrativo Nº 2081941 DE 2008 FONADE-UIS-ANH. http://oilproduction.net/files/cuencas%20petroleras%20de%20colombia-2009.pdf

Ghanizadeh, A., Clarkson, C., Aquino, S., Ardakani, O. & Sanei, H. (2015). Petrophysical and geomechanical characteristics of Canadian tight oil and liquid-rich gas reservoirs: I. Pore network and permeability characterization. *Fuel*, 153, 664–681. https://doi.org/10.1016/j.fuel.2015.03.020

Houseknecht, D.W. & Pittman, E.D. (1992). Origin, diagenesis & Petrophysics of Clay Minerals in Sandstones. *Special Publication 47. Society of Sedimentary Geologists, Tulsa*.

Jianfeng, T., Yongli, G. & Pengbo, Z. (2013). Genesis of illite in Chang 7 tight oil reservoir in Heshui area, Ordos Basin. *Oil and Gas Geology*, 34(5), 700-707.

Islam, M.A. (2009). Diagenesis and reservoir quality of Bhuban sandstones (Neogene), Titas Gas Field, Bengal Basin, Bangladesh. *Journal of Asian Earth Sciences*, 35(1), 89–100. https://doi.org/10.1016/j.jseaes.2009.01.006

Kantorowicz, J.D. (1990). The Influence of variations in illite morphology on the permeability of Middle Jurassic Brent Group sandstones, Cormorant Field, UK North Sea. *Marine and Petroleum Geology*, 7(1), 66-74. https://doi.org/10.1016/0264-8172(90)90057-N

Kareem, R., Cubillas, P., Gluyas, J., Bowen, L. & Greenwell, H.Ch. (2017). Multi-technique approach to the petrophysical characterization of Berea sandstone core plugs (Cleveland Quarries, USA). *Journal of Petroleum Science and Engineering*, 149, 436-455. https://doi.org/10.1016/j.petrol.2016.09.029

Kassab, M.A., Abu Hashish, M.F., Nabawy, B.S. & Elnaggar, O.M. (2017). Effect of kaolinite as a key factor controlling the petrophysical properties of the Nubia sandstone in central Eastern Desert, Egypt. *Journal of African Earth Sciences*, 125, 103-117. https://doi.org/10.1016/j.jafrearsci.2016.11.003

Kweon, H. & Deo, M. (2017). The impact of reactive surface area on brine-rock-carbon dioxide reactions in CO2 sequestration. *Fuel*, 188, 39-49. https://doi.org/10.1016/j.fuel.2016.10.010

Lai, J., Wang, G., Ran, Y. & Zhou, Z. (2015). Predictive distribution of high-quality reservoirs of tight gas sandstones by linking diagenesis to depositional facies: Evidence from Xu-2 sandstones in the Penglai area of the central Sichuan basin, China. *Journal of Natural Gas Science and Engineering*, 27, 810-822. https://doi.org/10.1016/j.jngse.2015.09.043

Loucks, R.G., Reed, R.M., Ruppel, S.C. & Hammes, U. (2012). Spectrum of pore types and networks in mudrocks and a descriptive classification for matrix-related mudrock pores. *AAPG Bulletin*, 96(6), 1071-1098. https://doi.org/10.1306/08171111061

Luffel, D.L., Hopkins, C.W. & Schettler, P.D. (1993). Matrix permeability measurements of gas productive shales. *Proceedings of the 68th Annual Technical Conference and Exhibition of the Society of Petroleum Engineers*, SPE 26633, Houston, USA.

Makhanov, K., Deutsch, C., Wong, R., Chan, J. & Payne, S. (2014). Modeling long-range channel deposits with a pattern-based approach. *Journal of Petroleum Science and Engineering*, 122, 678–693. https://doi.org/10.1016/j.petrol.2014.06.003

McKenny, B.J.L., Hamilton, P.J., Faiz, M. & Sayers, J. (2009). Mineralogical and petrophysical characterisation of coal seam gas reservoirs from the Bowen and Sydney basins, Australia. *International Journal of Coal Geology*, 79(3), 201-214. https://doi.org/10.1016/j.coal.2009.07.001

Nabawy, B.S. & Hossin, M. (2017). Statistical evaluation of the petrophysical controls on the effective porosity and permeability in heterogeneous sandstone reservoirs. *NRIAG Journal of Astronomy and Geophysics*, 6(1), 255-268. https://doi.org/10.1016/j.nrjag.2017.03.006

Nelson, P.H. (1994). Permeability-Porosity Relationships in Sedimentary Rocks. *Log Analyst*, 35(3), 38-62.

Potter, D.K. & Stephenson, A. (1988). Single-domain particles in rocks and magnetic fabric analysis. *Geophysical Research Letters*, 15(10), 1097-1100. https://doi.org/10.1029/GL015i010p01097

Rathnaweera, T.D., Ranjith, P.G., Perera, M.S.A. & Zhou, F. (2018). Characterisation of the effect of water saturation on the mechanical behaviour of reservoir rock using micro-computed tomography and acoustic emission techniques. *Marine and Petroleum Geology*, 91, 720-735. https://doi.org/10.1016/j.marpetgeo.2018.02.035

Rindel, A.K. & Chatterjee, R. (2016). Reservoir characterization of a tight gas sandstone reservoir using a multi-scale approach: a case study from Krishna Godavari basin, India. *Journal of Petroleum Science and Engineering*, 145, 157-173. https://doi.org/10.1016/j.petrol.2016.04.024

Schmidt, V. & McDonald, D.A. (1979). The role of secondary porosity in the course of sandstone diagenesis. *SEPM Special Publication*, 26, 175-207. https://doi.org/10.2110/pec.79.26.0175

Soto, J., Rueda, L., Zuluaga, L., Rueda, J., Sandoval, M., Achong, N., Reyes, A., Martínez, S., Torres, J., Vargas, J., Garzón, G. & Ladino, M. (2018). Evaluación del comportamiento de arenas arcillosas de Colombia en procesos de recuperación mejorada de hidrocarburos con inyección cíclica de CO2. *Revista Fuentes*, 16(2), 165-178. https://doi.org/10.18273/revfue.v16n2-2018008

Weibel, R. & Friis, H. (2007). Reservoir quality effects of diagenesis in feldspathic sandstones from the Lower Jurassic Gassum Formation, Norwegian–Danish Basin. *Geological Society, London, Special Publications*, 270(1), 95-110. https://doi.org/10.1144/GSL.SP.2007.270.01.07